IEEE Open Journal of
Power Electronics

Received 21 April 2021; revised 20 May 2021; accepted 27 May 2021. Date of publication 1 June 2021;
date of current version 23 June 2021. The review of this article was arranged by Associate Editor Gab-Su Seo.

Digital Object Identifier 10.1109/OJPEL.2021.3085863

Unified Fast-Dynamic Direct-Current Control Scheme for Intermediary Inductive AC-Link Isolated DC-DC Converters

NIE HOU (Student Member, IEEE), YUZHOU LI (Student Member, IEEE), ZHONGYI QUAN (Member, IEEE), YUN WEI LI (Fellow, IEEE), AND ANDREW ZHOU

Department of Electrical and Computer Engineering, University of Alberta, Edmonton, AB T6G 1H9, Canada

CORRESPONDING AUTHOR: YUZHOU LI (e-mail: yuzhuo@ualberta.ca)

This work was supported by Future Energy Systems research initiative by Canada First Research Excellence Fund and Alberta Innovates

ABSTRACT The isolated dc-dc converters with middle inductive AC links dc-dc converter have been extensively studied in modern energy conversion applications for safety and reliability, especially those featuring intermediary inductive ac-link (I^2ACL) configurations such as full-bridge dc-dc converter and dual-active-bridge (DAB). However, up to now, the dynamic equivalence in these I^2ACL type converters has not been systematically revealed. To fill such a gap, in this paper, the existing I^2ACL isolated dc-dc converters are reviewed thoroughly, including unidirectional type and bidirectional type. Then, the general current transferred features of these two groups are analyzed, respectively, and the transferred current during the transient process is just influenced by the middle inductance little. So, the I^2ACL isolated dc-dc converter can be regarded as the first-order converter. Based on the discovered general characteristic, a unified fast-dynamic direct-current (FDDC) control scheme is proposed for improving the dynamic performance of these I^2ACL isolated dc-dc converters. Such a scheme can also facilitate the uniform control design for existing or emerging new topologies with the same electrical equivalence. Moreover, the specialized design principles of the PI parameters in the unified FDDC control method are also presented. Finally, to verify the universality and feasibility of the proposed general FDDC control strategy, both simulation and experiment results are presented with demonstration examples, e.g., full-bridge type, DAB-type, and the three-phase DAB type dc-dc converters.

INDEX TERMS Fast dynamic response, full bridge converter, DAB converter, three-phase DAB converter.

I. INTRODUCTION

Isolated dc-dc converters have been extensively applied in modern industrial applications such as metro vehicles [1], electric vehicles [2]–[4], data center [5], and grid systems [6]–[9], etc. Real-world projects can be found like the auxiliary power supply of a metro vehicle system shown in Fig. 1, where the isolated dc-dc power conversion stage is employed to replace the traditional line-frequency for lower cost, smaller size, and less acoustic noise [1]. Or the utility-service equipment like the back-to-back converter system as shown in Fig. 2, which is embedded with isolated dc-dc converters to solve the power flow balancing problems with asynchronized ac grids [8]. In addition, given the great potentials of dc microgrids over conventional ac configurations, more isolated dc-dc converters can be expected to be employed with galvanic isolation and flexible voltage turning ability (an example is shown in Fig. 3).

In practice, galvanic isolation is required mainly for safety and grounding reasons. The isolated structures offer great flexibility of various grounding techniques on both dc sides, as well as easier parallel or series connections [10], [11]. Therefore, the same elementary cells can be modularly implemented in the power converter stage with much easier scalability regarding power and voltage ratings. In such a way, the inherent dc-fault blocking capability can be acquired naturally since the intermediary ac power stage is embedded in the isolated dc-dc stage [12]–[13]. Moreover, the intermediary transformer provides high flexibility for connecting two dc

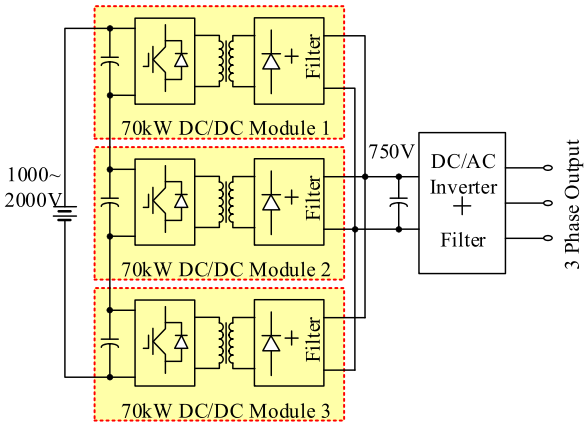

FIGURE 1. **Overall system configuration of 210kW auxiliary power supply for metro vehicle system [1].**

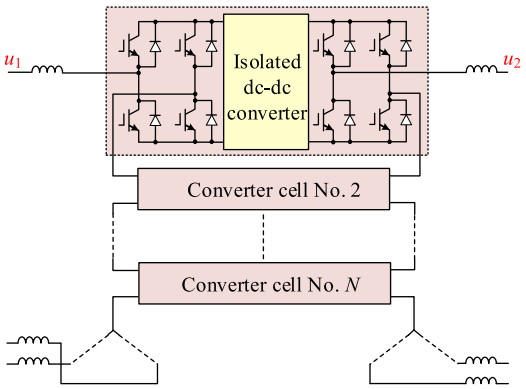

FIGURE 2. **The 6.6 kV back-to-back system in the next-generation medium-voltage power conversion system [8].**

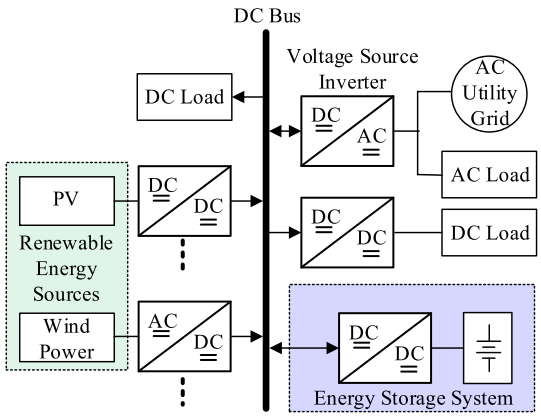

FIGURE 3. **The typical dc microgrid system [9].**

buses with large voltage differences. Therefore, isolated dc-dc converters can serve as universal solutions for applications covering various voltage ratings.

Based on different criterion, isolated dc-dc converters can be classified into different types such as resonant/non-resonant dc-dc converters [14]–[15], voltage-source/current-source/impedance-source dc-dc converters [16], etc.

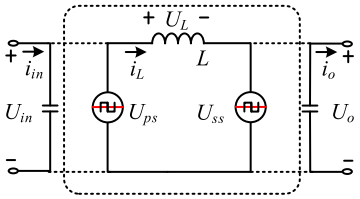

FIGURE 4. **The simplified circuit of one power transferring branch in the I²ACL isolated dc-dc converter.**

In recent years, non-resonant isolated dc-dc converters have drawn some great attention in both academic and industry, e.g., full-bridge (FB) dc-dc converter [17], dual-active bridge (DAB) dc-dc converter [18], and their variant topologies [19]–[22]. Without losing generality, the simplified circuit of one power-transferred branch in the above dc-dc converters can be modeled in a universal way as shown in Fig. 4, which indicates a strong dynamic equivalence among these converters. However, up to now, such electrical equivalence has not been discovered in the isolated dc-dc converter research field, let alone the unified fast-dynamic control method.

To fill such a gap, in this paper, a thorough overview of existing isolated dc-dc converters is presented. To better capture the core features of power transferring in this kind of isolated dc-dc converter, it will be called an intermediary inductive ac-link (I^2ACL) isolated dc-dc converter in this work. The topologies are divided into two basic types including unidirectional I^2ACL dc-dc converter and bidirectional I^2ACL dc-dc converter. In the following Section II, switching networks that can form various I^2ACL dc-dc converters are analyzed, and then, the existing unidirectional and bidirectional I^2ACL dc-dc converters are reviewed and classified. Then, in Section III, a unified fast-dynamic direct-current (FDDC) control scheme is proposed for these converters for improving the dynamic response under the disturbance of input voltage and load conditions. And the design principle of the PI parameters is also presented. In Section IV, the simulation and experimental results are provided to validate the effectiveness of the presented strategy by using the full-bridge dc-dc converter, the DAB dc-dc converter, and the three-phase DAB dc-dc converter as examples. Finally, the paper is concluded with Section V.

II. TOPOLOGIES AND EQUIVALENT MODELS OF MIDDLE INDUCTIVE AC-LINK ISOLATED DC-DC CONVERTERS

In terms of power transferring stages, the I^2ACL dc-dc converter can be divided into the dc-ac stage and the ac-dc stage. Generally, the voltage-fed switching networks are required to obtain ac voltage from dc voltage, then the energy conversion between dc power and ac power can be realized. Thus, the potential building blocks of the I^2ACL dc-dc converter are analyzed firstly in this Section. Then, based on these blocks, the existing unidirectional I^2ACL dc-dc converters and bidirectional I^2ACL dc-dc converters are reviewed.

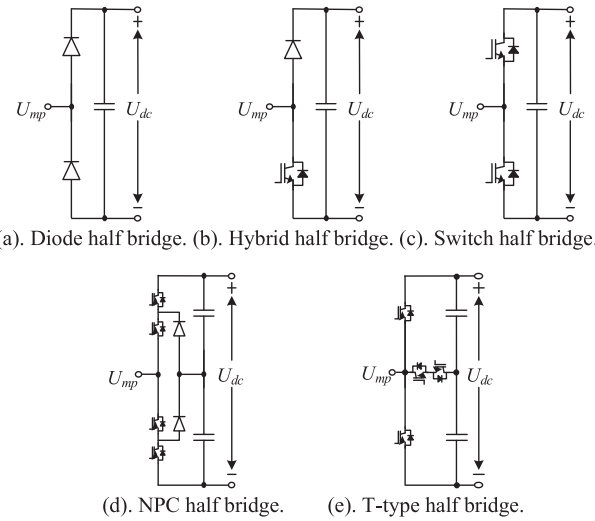

(a). Diode half bridge. (b). Hybrid half bridge. (c). Switch half bridge.

(d). NPC half bridge. (e). T-type half bridge.

FIGURE 5. The basic half bridges for establishing the switching network for I²ACL dc-dc converter.

A. THE POTENTIAL HALF BRIDGES FOR THE I²ACL ISOLATED DC-DC CONVERTER

The existing half bridges which can be employed to build the I²ACL isolated dc-dc Converters are demonstrated in Fig. 5. Five types can be considered, including the diode-based half bridge, hybrid half bridge, switch-based half bridge, neutral point clamped (NPC) half bridge [23], and T-type half bridge [24]. (It is noted for interested readers that other switching networks can also be employed to obtain ac voltage from dc voltage, such as multilevel NPC bridge [25] and active NPC bridge [26], etc.) As shown in Fig. 5, the first three half bridges can usually achieve two voltage levels as 0 and U_{dc}, and the latter two half bridges can usually achieve three voltage levels as 0, $U_{dc}/2$, and U_{dc}. Then, based on these half bridges, different switching networks can be obtained for forming ac voltage.

Basically, combing the series capacitors and the half bridge, the simplest bridges that can be obtained for acquiring the ac output voltage is shown in Fig. 6. The first three bridges can obtain the ac voltage by $-U_{dc}/2$ and $U_{dc}/2$, and the latter two bridges can generate the ac voltage by $-U_{dc}/2$, 0, and $U_{dc}/2$. Since these bridges are constructed by one half bridge in Fig. 5, the I²ACL dc-dc converter constructed by these bridges can be called half-bridge dc-dc converter.

Moreover, based on any two half bridges in Fig. 5, the full bridges can be acquired. Then, the full bridges with the same half bridge are shown in Fig. 7, which are the most used full bridges for establishing the existing isolated dc-dc converters. Compared with the first three H bridges, the latter two H bridges including the NPC full bridges and the T-Type full bridges can generate multi-level ac voltages, and the I²ACL dc-dc converters established by the latter two full bridges are usually called multi-level dc-dc converters. Some I²ACL isolated dc-dc converters are established by the full bridges

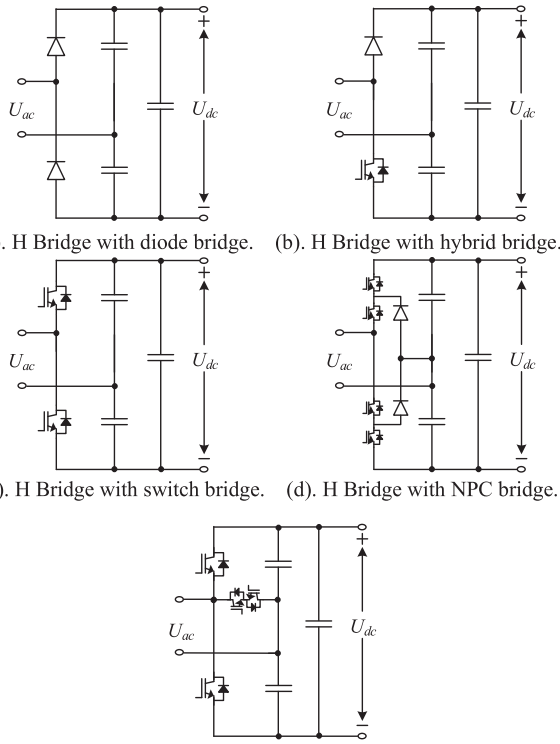

(a). H Bridge with diode bridge. (b). H Bridge with hybrid bridge.

(c). H Bridge with switch bridge. (d). H Bridge with NPC bridge.

(e). H Bridge with T-type bridge.

FIGURE 6. The switching network with one half bridge for forming ac voltage.

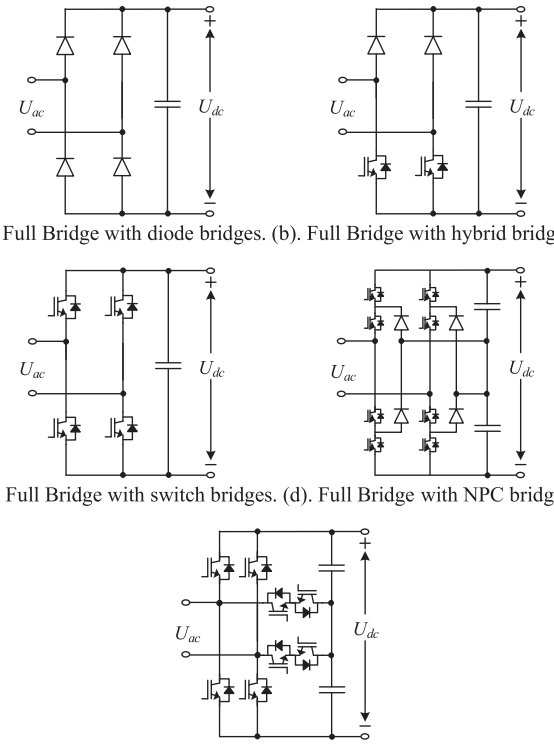

(a). Full Bridge with diode bridges. (b). Full Bridge with hybrid bridges.

(c). Full Bridge with switch bridges. (d). Full Bridge with NPC bridges.

(e). Full Bridge with T-type bridges.

FIGURE 7. The switching network with two half bridges for I²ACL dc-dc converter.

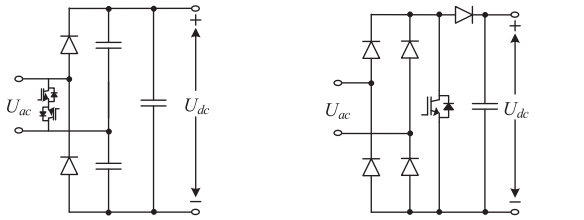

FIGURE 8. The switching network based on diode half Bridges embedded with zero-level voltage.

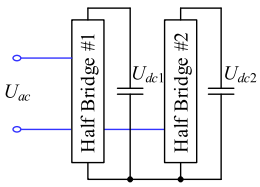

FIGURE 9. The full Bridge with different dc-link voltages.

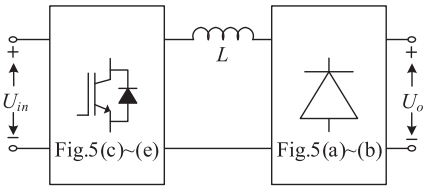

FIGURE 10. The simplified circuit of unidirectional I^2ACL dc-dc converters.

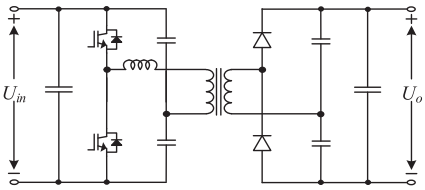

FIGURE 11. The topology of the asymmetric half-bridge dc-dc converter with diode half bridge [31].

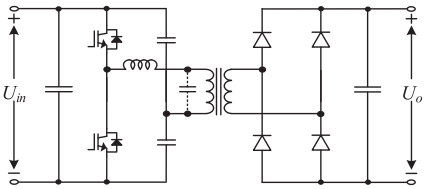

FIGURE 12. The topology of the asymmetric half-bridge dc-dc converter with diode full bridge [31].

with different half bridges, and these full bridges will be mentioned in the review of the specific I^2ACL dc-dc converters. Similarly, with multiple half bridges, the multi-phase I^2ACL dc-dc converter can be acquired.

In addition, when only diodes are employed to establish the H bridges as shown in Fig. 7(a), zero level voltage cannot be provided, which usually limits the voltage range of I^2ACL dc-dc converters with these diode-based H bridges. Thus, diode-based H bridges with extra switches are required to boost the output range of these I^2ACL dc-dc converters as shown in Fig. 8.

Notably, although the half bridges (shown in Figs. 6–Fig. 8) usually acquire voltage from the same dc bus or capacitor, these half bridges in the same H bridges can connect with different dc buses as shown in Fig. 9, which may be suitable for applications with multi-port sources.

B. THE UNIDIRECTIONAL I^2ACL ISOLATED DC-DC CONVERTER

In this part, the existing unidirectional I^2ACL dc-dc converters are reviewed, and the simplified circuit of one branch of these converters can be expressed as shown in Fig. 10, where the primary side of the unidirectional I^2ACL dc-dc converter is established by the controllable switches as shown in Figs. 5(c)–Fig. 5(e), and the secondary side of the unidirectional I^2ACL dc-dc converter is constructed by the uncontrollable diodes as shown in Figs. 5(a)–Fig. 5(b). Since diodes can only deal with the unidirectional power flow, the power of the unidirectional I^2ACL dc-dc converter can only be transferred from the primary side to the secondary side. Then, the unidirectional I^2ACL dc-dc converter is usually employed to connect the renewable sources and the dc links such as photovoltaic system or fuel cell system for maximum power point tracking performance [27], [28], and when the unidirectional I^2ACL dc-dc converter is connected to power consumer side, this converter can also be used to adjust the dc-link voltage [29], [30].

Simply, combining the switching networks as shown in Fig. 6(a) and Fig. 6(c), the asymmetric half bridge dc-dc converter with diode half bridge can be obtained as shown in Fig. 11 [31]. Further, by switching the secondary-side H Bridge to the diode full bridge as shown in Fig. 7(a), the asymmetric half bridge dc-dc converter with diode full bridge can be acquired as shown in Fig. 12 [31]. Similarly, by switching the primary-side H Bridge to the switch full bridge as shown in Fig. 7(c), the full bridge dc-dc converter with diode half bridge can be shown in Fig. 13 [32]. Then, combining the switch full bridge and the diode full bridge, the full bridge dc-dc converter with diode full bridge can be generated as shown in Fig. 14 [33], which may be the most popular unidirectional isolated dc-dc converter in industrial applications.

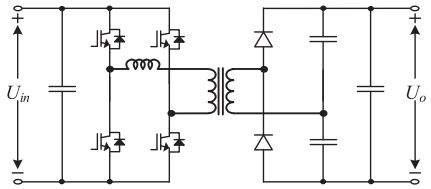

FIGURE 13. The topology of the full bridge dc-dc converter with diode half bridge [32].

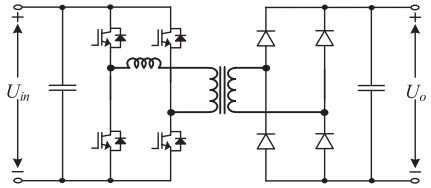

FIGURE 14. The topology of the full bridge dc-dc converter with diode full bridge [33].

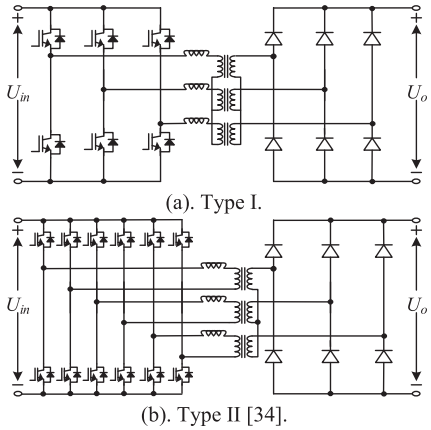

FIGURE 15. The topology of the three-phase dc-dc converters with diode three-phase bridge.

Moreover, when the primary side and the secondary side both have three half bridges, the three-phase unidirectional dc-dc converter with three-phase diode bridge can be obtained as shown in Fig. 15(a). By switching the primary-side three-phase bridge to three dual active bridges, another three-phase unidirectional dc-dc converter can be obtained as shown in Fig. 15(b) [34].

Since the secondary-side bridges of the topologies as shown in Figs. 11–Fig. 15 are only established by the diodes, these bridges cannot provide zero voltage, which usually limits the output-voltage range of these converters. Therefore, some extra switches can be employed to boost the output range of these converters, and the potential bridges can be selected from Fig. 7(b) and Fig. 8. Then, the full-bridge dc-dc converters with active boost rectifier are shown in Fig. 16. Similarly, as shown in Fig. 18, a three-phase semi-dual active bridge dc-dc converter is presented for wide input variations and high voltage interface [37].

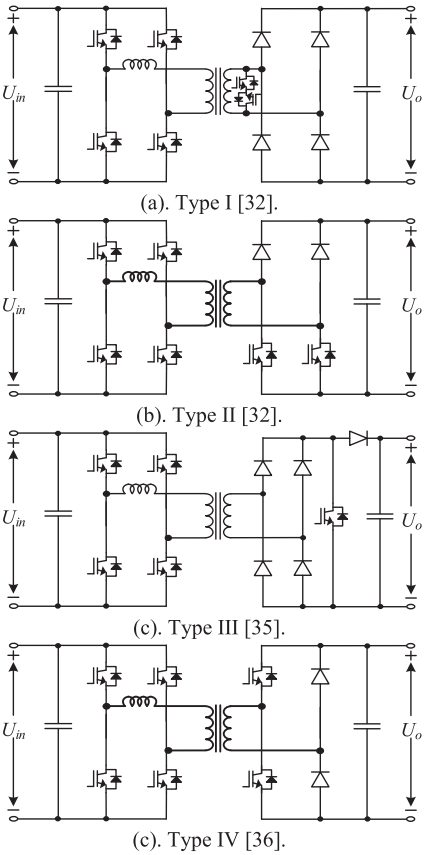

FIGURE 16. The topologies of single-phase unidirectional I^2ACL dc-dc converters with active boost rectifier.

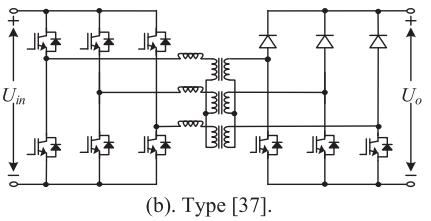

FIGURE 17. The topologies of three-phase unidirectional I^2ACL dc-dc converters with active boost rectifier.

In addition, as shown in Fig. 9, the half bridges in the same switching network can be connected to different dc links, which can be employed in multiple-port converter system and can be used to generate multiple-level voltages. Then, a secondary-side modulated full-bridge dc-dc converter is shown in Fig. 18(a) [38]. However, this full-bridge dc-dc converter cannot generate symmetrical three-level voltages on the secondary side, the modified secondary-side modulated full-bridge dc-dc converters can be shown in Fig. 18(b) [39].

With electrical isolation, the unidirectional I^2ACL dc-dc converter can be easily designed as a module with parallel or series configurations for high-power and high-voltage applications, especially one-side parallel and one-side series [19].

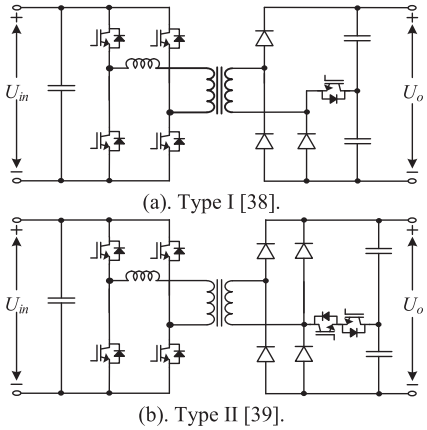

FIGURE 18. The topology of the secondary-side modulated full bridge dc-dc converter.

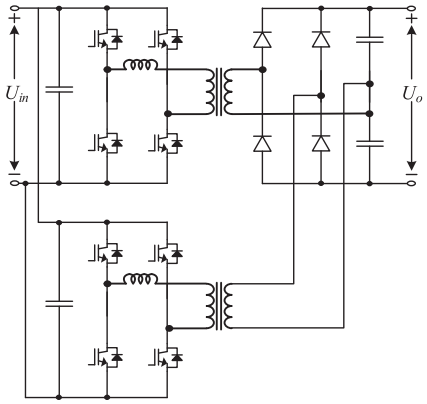

FIGURE 19. Interleaved full-bridge converter with diode half bridges [40].

There are also some variant unidirectional I^2ACL dc-dc converters with multiple H bridges for high-power high-voltage applications. An interleaved full-bridge converter with diode half bridges can be shown in Fig. 19 [40], and a full-bridge dc-dc converter with paralleled input IGBTs and split secondary windings can be shown in Fig. 20 [41].

C. THE BIDIRECTIONAL I^2ACL ISOLATED DC-DC CONVERTER

In this part, the existing bidirectional I^2ACL dc-dc converters are reviewed, and the simplified circuit of one branch of this kind of converter can be expressed as Fig. 21, where both the primary side and the secondary side of these converters are constructed with controllable half bridges as shown in Figs. 5(c)–;Fig. 5(e). Based on two half switch bridges, the symmetrical half-bridge dc-dc converter can be shown in Fig. 22 [42]. Then, by changing the primary-side H Bridge as the dual active bridge, the unsymmetrical dual active bridge dc-dc converter can be shown in Fig. 23 [43]. Moreover, when both sides are dual active bridges, the dual active bridge dc-dc converter can be acquired as shown in Fig. 24 [44], which is regarded as one of the most promising dc-dc converters.

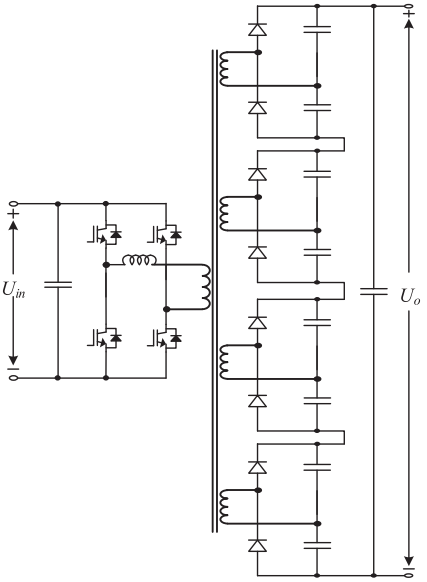

FIGURE 20. Full-bridge converter with paralleled input IGBTs and split secondary windings [41].

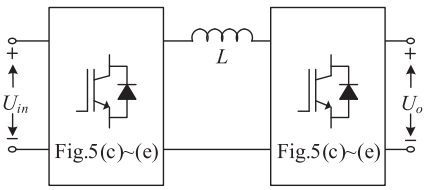

FIGURE 21. The simplified circuit of bidirectional I^2ACL dc-dc converters.

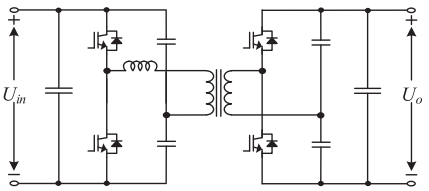

FIGURE 22. The topology of the symmetrical half-bridge dc-dc converter [42].

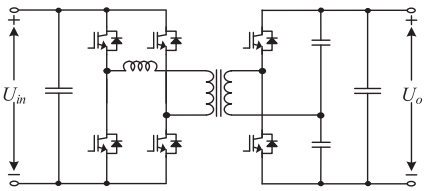

FIGURE 23. The topology of the unsymmetrical dual-active-bridge dc-dc converter with switch half bridge [43].

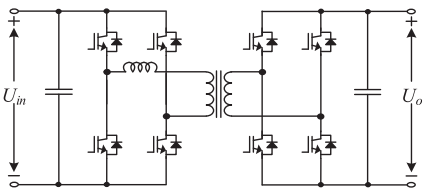

FIGURE 24. The topology of the dual active bridge dc-dc converter [44].

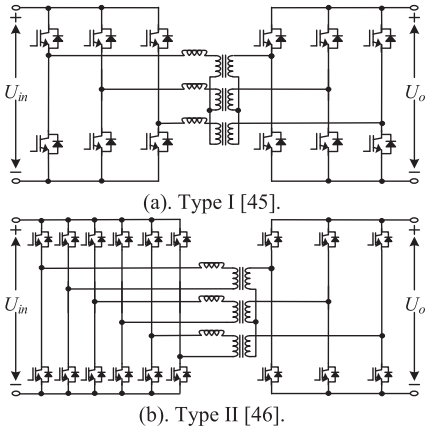

FIGURE 25. The topology of the three-phase dual active bridge dc-dc converters.

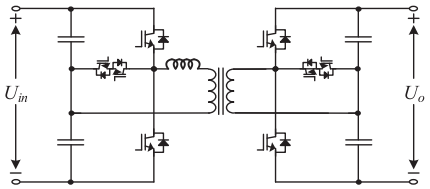

FIGURE 26. The topology of the three-level symmetrical T-type dc-dc converter [47].

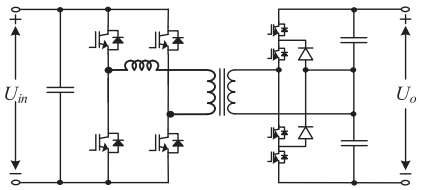

FIGURE 27. The topology of the three-level unsymmetrical NPC dc-dc converter [48].

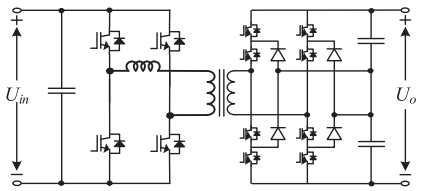

FIGURE 28. The topology of the five-level unsymmetrical NPC dc-dc converter [49].

Similarly, when the primary side and the secondary side both have three half bridges, the well-known three-phase dual-active bridge dc-dc converter can be shown in Fig. 25(a) [45]. Then, by switching the primary-side three-phase bridge as three dual active bridges, another three-phase bidirectional dc-dc converter can be obtained as shown in Fig. 25(b) [46].

Moreover, based on T-type half bridge and NPC half bridge as shown in Fig. 5(d) and Fig. 5(e), some multilevel isolated dc-dc converters can be obtained as shown in Figs. 26–Fig. 29. Combining two T-type half bridge, a three-level symmetrical

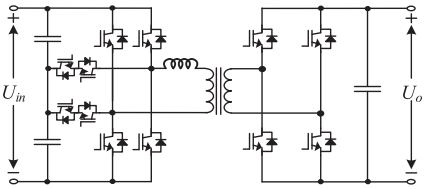

FIGURE 29. The topology of the five-level unsymmetrical T-type dual active bridge dc-dc converter [50].

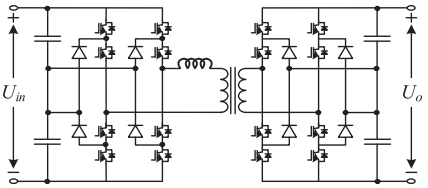

FIGURE 30. The topology of the five-level symmetrical NPC dc-dc converter [51].

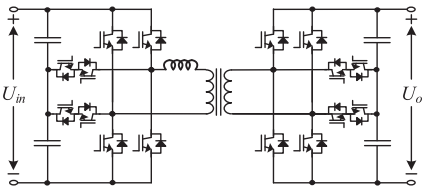

FIGURE 31. The topology of the five-level symmetrical T-type dc-dc Converter.

T-type isolated dc-dc converter can be shown in Fig. 26 [47], which has a smaller number of switches. Then, by combing the NPC half bridge and the full bridge, a three-level unsymmetrical NPC dc-dc converter can be shown in Fig. 28 [48], which can be employed to connect the low voltage bus and the high voltage bus. Moreover, combining the full bridge and the full NPC bridge, the five-level unsymmetrical NPC dc-dc converter can be obtained as shown in Fig. 28 [49]. By switching the full NPC bridge to the T-type bridge, the five-level unsymmetrical T-type DAB dc-dc converter can be obtained as shown in Fig. 29 [50]. Then, combining two full NPC bridges, the five-level symmetrical NPC dc-dc converter can be obtained as shown in Fig. 30 [51], which is a promising candidate for the high voltage dc-dc applications. Similarly, the five-level symmetrical T-type dc-dc converter can be obtained as shown in Fig. 31.

In addition, based on multiple-winding transformers and different half bridges, some I^2ACL dc-dc converters can be obtained as shown in Figs. 32–Fig. 34, which is usually employed to reduce the current stress of the switches or increase the power density of the converter system. As shown in Fig. 32, a three-winding-transformer-based dual active bridge dc-dc converter is presented for reducing the current stress of switches on the secondary side [52]. Moreover, a multi-winding-transformer-based dual active bridge dc-dc converter with paralleled output configuration can be shown in Fig. 33, which can be employed to reduce the current stress at the

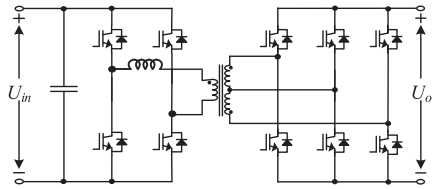

FIGURE 32. The three-winding-transformer-based dual active bridge dc-dc converter [52].

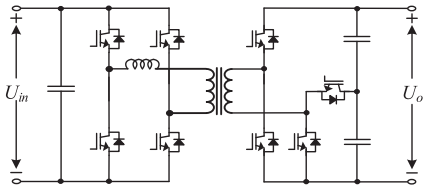

FIGURE 35. The topology of the secondary-side modulated bidirectional full-bridge dc-dc converter [38].

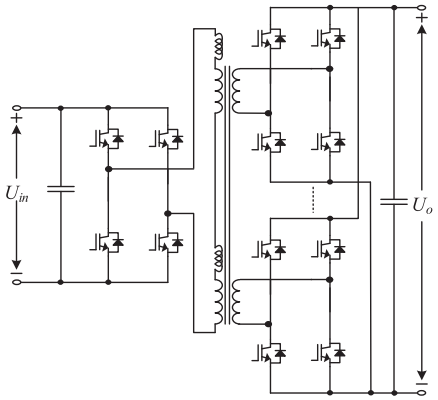

FIGURE 33. The multi-winding-transformer-based dual active bridge dc-dc converter with paralleled output configuration [53].

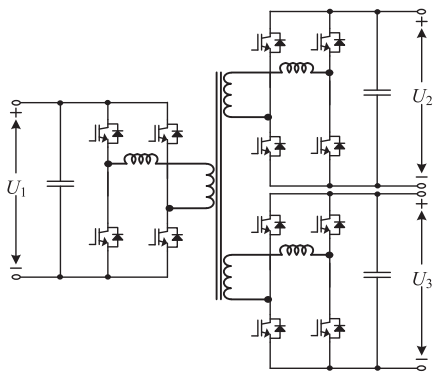

FIGURE 34. The three-port dual active bridge dc-dc converter [20].

low-voltage side when the difference between the input voltage and the output voltage is very large [53]. Then, based on the three-winding transformer, a three-port dual active bridge dc-dc converter can be obtained for arranging the power transmission among three independent dc terminals as shown in Fig. 34 [20].

As shown in Fig. 9, the half bridges in the same switching network can be connected to different dc links, which can be employed in the multi-port converter system and can be used to generate multiple-level voltages. Similarly, a secondary-side modulated bidirectional full-bridge dc-dc converter can be shown in Fig. 35 [38].

C. THE SUMMARY OF THE UNIDIRECTIONAL AND BIDIRECTIONAL I²ACL ISOLATED DC-DC CONVERTER

Based on the previous overview, these existing unidirectional and bidirectional I^2ACL isolated dc-dc converters can be summarized in Fig. 36. Based on the voltage level, the phase number, and the winding number, these existing topologies are divided into five categories including two-level I^2ACL converter, three-level I^2ACL converter, multi-level I^2ACL converter, multi-phase I^2ACL converter, and multi-winding I^2ACL converter.

Generally, the unidirectional I^2ACL dc-dc converter can be employed in some unidirectional applications such as PV and fuel cell systems [31]–[41]. The bidirectional I^2ACL dc-dc converter can be used in some bidirectional applications such as energy storage systems and dc grid systems [20], [42]–[53]. According to the voltage value, the two-level I^2ACL isolated dc-dc converter and the three-level I^2ACL isolated dc-dc converter can be employed in some low voltage conditions [33], [35], [42], [47]. Since the multi-level I^2ACL isolated dc-dc converter can tolerate higher voltage, these converters can be suitable for some middle voltage applications [49], [50]. Moreover, compared with the single-phase I^2ACL isolated dc-dc converter, the multi-phase I^2ACL isolated dc-dc converter can provide a lower ripple current to the dc-link [37], [46], so a lower dc-link capacitor can usually be adopted. Sometimes, multi-ports may be required for connecting several voltage sources, where the multi-winding I^2ACL isolated dc-dcconverters can be used for high power density [20], [41], [53]. Compared with the single-phase two-winding I^2ACL isolated dc-dc converters, the transformer design of the last two types will be usually more difficult.

III. THE PROPOSED UNIFIED FAST-DYNAMIC CONTROL SCHEME FOR I²ACL DC-DC CONVERTER

In this Section, the unified FDDC control scheme will be proposed for improving the dynamic response of the I^2ACL isolated dc-dc converter when the input voltage and the load condition are suddenly changed. As shown in Fig. 4, there is always a middle inductance in one power transferring branch of the I^2ACL dc-dc converters, so the influence on the transient process will be analyzed first in this Section. Then, the order reducing phenomenon of the I^2ACL dc-dc converter can be obtained since the middle inductance can only influence the transient process a little. Moreover, based on this characteristic, a unified FDDC control scheme is proposed for all the

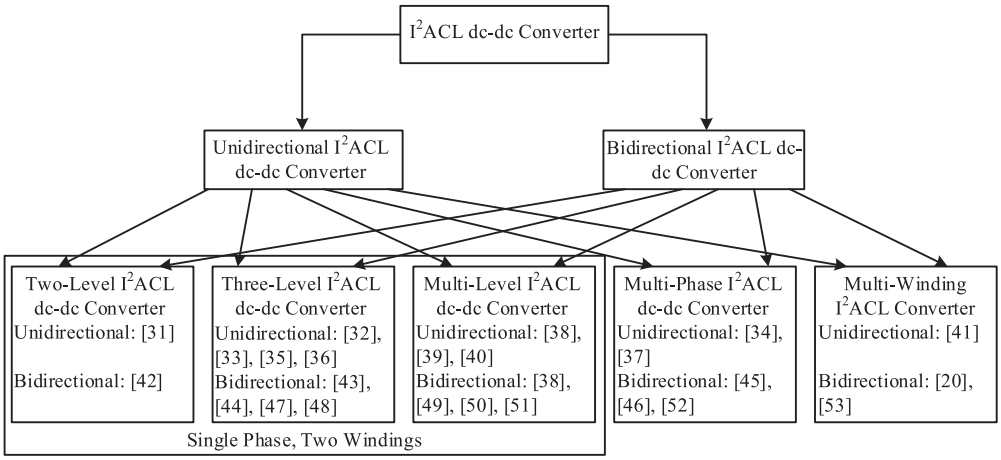

FIGURE 36. Detailed classification of the existing I²ACL isolated dc-dc converters.

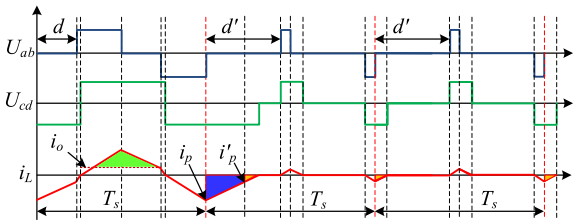

FIGURE 37. The transient waveforms when the transferred power of the full-bridge dc-dc converter is changed.

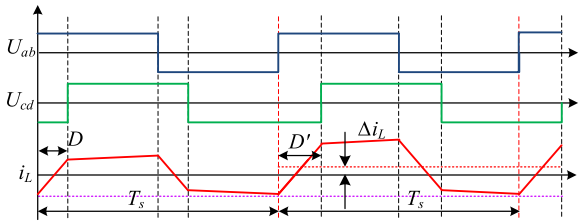

FIGURE 38. The transient waveforms when the transferred power of the DAB dc-dc converter is changed.

I²ACL dc-dc converters with the design principle of PI parameters. In addition, since the large efficiency difference will usually influence the proposed general fast-dynamic control strategy, a compensation operation for efficiency difference will be presented for ensuring the dynamic response of the proposed FDDC control scheme.

A. THE POWER TRANSFERRED CHARACTERISTICS OF I²ACL ISOLATED DC-DC CONVERTER

From the previous analysis, there are two kinds of I²ACL dc-dc converters including the unidirectional I²ACL dc-dc converter and the bidirectional I²ACL dc-dc converter. Different from the unidirectional I²ACL dc-dc converter, both sides of the bidirectional I²ACL dc-dc converter can be positively controllable. So, in terms of the transient performance when the transferred power of the converter is suddenly changed for dealing with the disturbance of input voltage and load condition, there is a little difference between the unidirectional I²ACL dc-dc converter and the bidirectional I²ACL dc-dc converter. By using the full-bridge dc-dc converter as an example for the unidirectional I²ACL dc-dc converter, when the transferred power is suddenly changed with the disturbance of input voltage and load condition, the transient waveforms of the full-bridge dc-dc converter can be shown in Fig. 37.

As shown in Fig. 37, when the required transferred power of the full bridge is suddenly changed, the required transferred power can be usually obtained in the second switching period when the phase-shift ratio d is changed. Moreover, in the first switching period, there is additional power stored in the middle inductance, which is transferred from the input side to the output side. The additional power P_a can be calculated as,

$$P_a = \frac{L(i_p^2 - i_p'^2)}{2T_s} \tag{1}$$

where i_p and $i_p^{'}$ are the peak currents of the middle inductance before and after the disturbance of phase-shift ratio d, respectively. Then, the output-voltage disturbance ΔU_o caused by the additional power can be expressed as,

$$\Delta U_o \approx \frac{L(i_p^2 - i_p'^2)}{2C_o U_o} \tag{2}$$

As shown in Fig. 37, the green part of the middle-inductance current usually results in the output-voltage ripple. So, output-voltage disturbance ΔU_o caused by the additional power from the middle inductance is usually similar to the output-voltage ripple, and this additional power cannot influence the transient performance of the full-bridge dc-dc converter.

Moreover, by using the DAB dc-dc converter as an example for bidirectional I²ACL dc-dc converter, when the transferred power suddenly changes for addressing the disturbance of input voltage and load condition, the transient waveforms of the DAB dc-dc converter can be shown in Fig. 38.

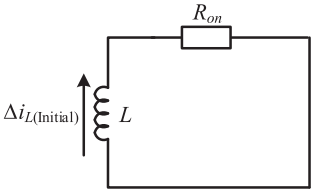

FIGURE 39. The equivalent circuit for the dc offset of the inductance current at the steady-state condition.

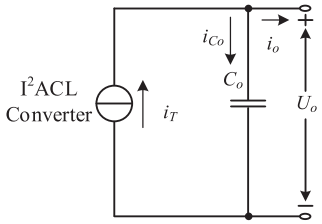

FIGURE 40. The simplified circuit of the I²ACL dc-dc converter.

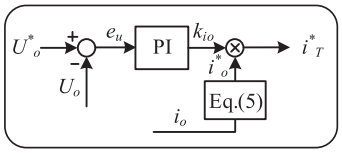

FIGURE 41. The diagram for obtaining the actual required transferred current i^*_T.

As shown in Fig. 38, since the input voltage and the output voltage can be regarded as the same in a switching period, the transferred power P_T of the DAB dc-dc converter can be calculated by the new phase-shift ratio D' as,

$$\begin{aligned} P_T &= \frac{1}{T_s}\int_0^{T_s}\frac{U_{cd}}{n}(i_L+\Delta i_L)dt = \frac{1}{T_s}\int_0^{T_s}U_{ab}(i_L+\Delta i_L)dt \\ &= \frac{2}{T_s}\int_0^{\frac{T_s}{2}}U_{in}i_L dt + \frac{\Delta i_L}{T_s}\int_0^{T_s}U_{ab}dt \\ &= \frac{2}{T_s}\int_0^{\frac{T_s}{2}}U_{in}i_L dt = \frac{U_{in}U_o D(1-D)T_s}{2nL} \end{aligned} \tag{3}$$

According to (3), since the dc offset current of the middle inductance cannot influence the power transmission of the DAB dc-dc converter, the transferred power of the DAB dc-dc converter can be controlled by the phase-shift ratio accurately at the steady-state condition and during the transient process [54]. In addition, the dc offset of the inductance current can be consumed by the conducting resistor R_{on} of the DAB dc-dc converter, and since U_{ab} and U_{cd} are total ac components at steady state condition which cannot generate dc inductance current, the equivalent circuit can be shown as Fig. 39. Then, the dc offset of the inductance current Δi_L can be consumed by the conducting resistor R_{on} of the DAB dc-dc converter gradually, which affects the transferred power of this converter slightly with the tiny conducting resistor.

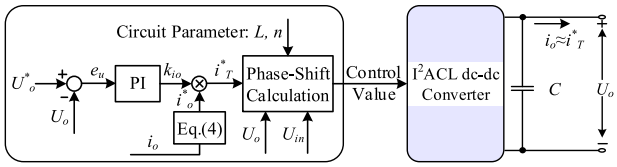

FIGURE 42. The diagrams of the unified FDDC control schemes for the I²ACL dc-dc converter.

Therefore, for the I²ACL dc-dc converter including the unidirectional I²ACL dc-dc converter and the bidirectional I²ACL dc-dc converter, when the transferred power is suddenly changed for dealing with the variation of input voltage and load condition, the required transferred power can be obtained within two switching periods. Then, the required transferred current of the I²ACL dc-dc converter can be calculated as,

$$i_T = \frac{P_T}{U_o} \tag{4}$$

In (4), since output voltage can remain at its desired value with the sudden change of suitable transferred power, the required transferred current can also be obtained within two switching periods for a certain phase-shift ratio. Then, the transferred current i_T of the I²ACL converter can be directly controlled by the phase-shift value timely. With current-level modulation, the I²ACL dc-dc converter can be regarded as the controllable current source [55], and the simplified circuit of the I²ACL isolated dc-dc converter can be demonstrated in Fig. 42. So, although there is the middle inductance in the I²ACL isolated dc-dc converter, the middle inductance will not influence the transient performance of this kind of converter, which is very different from the traditional dc-dc converters such as BUCK and BOOST. Based on this characteristic, the order reducing phenomenon can be obtained, and the fast-dynamic performance can be easily provided for the I²ACL dc-dc converter.

B. THE UNIFIED FAST-DYNAMIC DIRECT-CURRENT CONTROL METHOD FOR I²ACL ISOLATED DC-DC CONVERTER

Based on the power or current transferring characteristic of I²ACL dc-dc converters previously, a general FDDC control method will be proposed for this type of converters, which can be employed to deal with the variations of the input voltage and the load condition. To face the load-condition change, the load current can be measured to calculate the desired output current i^*_o as,

$$i^*_o = \frac{U^*_o}{R} = \frac{i_o U^*_o}{U_o} \tag{5}$$

where R is the load equivalent resistor. Then, based on Energy Conversion Law, the required transferred current of the I²ACL dc-dc converter should be the same as the desired output current. However, there are always some power losses in the converter system, which will result in a little difference

between the transferred current and the output current. So, the voltage deviation will be unavoidable. In order to compensate for the error caused by the power loss and other uncertain values, the PI controller is used for obtaining a compensation coefficient k_{io} for acquiring the actual required transferred current. Then, the diagram for obtaining the actual required transferred current i^*_T can be shown in Fig. 41.

Moreover, the phase-shift modulation method is the most popular modulation method for the I^{2}ACL dc-dc converter, and based on the phase-shift ratio, the transferred current of these dc-dc converters can be directly obtained [8]. In reverse, when the required transferred current is obtained, the phase-shift ratio can be calculated. Then, the complete diagram of the unified FDDC control method for the I^{2}ACL dc-dc converter can be shown in Fig. 42.

As shown in Fig. 42, the general FDDC control scheme can be realized for the I^{2}ACL dc-dc converter. At the beginning of each switching period, the input voltage U_{in}, the output voltage U_o and the load current i_o are measured. Based on the PI controller, the compensation factor k_{io} can be obtained by the output voltage U_o and its desired value U^*_o. Then, according to (5), the required load current i^*_o can be calculated by the actual load current i_o, the output voltage U_o and its desired value U^*_o. Moreover, by combining the compensation factor k_{io} and the required load current i^*_o, the required transferred current i^*_T of the I^{2}ACL dc-dc converter can be obtained. Then, based on the relationship between the transferred current i_T and the phase-shift ratio of the I^{2}ACL dc-dc converter, the required phase-shift ratio can usually be obtained by using the circuit parameter, the output voltage U_o, the input voltage U_{in} and the required transferred current i^*_T. Finally, based on the phase-shift modulation part, the required transferred current i^*_T can be realized, which can meet the requirement of the load consumption. Then, the ultrafast dynamic response can be provided for the I^{2}ACL dc-dc converter when the input voltage and load condition are changed, and, since the compensation part is multiplied with the feed-forward load current, this unified FDDC control scheme is not sensitive to the circuit parameter [30], [54].

C. THE DESIGN PRINCIPLE OF PI PARAMETERS

As shown in Fig. 41, when the transferred power of the I^{2}ACL dc-dc converter is controlled by the phase-shift ratio accurately and timely, the middle inductance can be omitted in its simplified circuit. Then, only the output capacitor will influence the dynamic performance of the I^{2}ACL dc-dc converter, and the dynamic model of the output capacitor can be expressed as,

$$C_o \frac{dU_o}{dt} = i_T - i_o \tag{6}$$

Based on the proposed general fast-dynamic control scheme, the transferred current of the I^{2}ACL dc-dc converter can meet the requirement of the load condition immediately, and according to (6), the disturbance of output voltage during the transient process will be limited. Therefore, the PI parameters in the general fast-dynamic control scheme cannot be determined based on the transient process, which is different from the traditional way of designing the PI parameter.

Moreover, when the measurement noise is considered, there should be irregular oscillations in phase-shift ratio at steady-state conditions, which may result in the irregular oscillations of output voltage. With the filter function of the output capacitor, the oscillation of the output voltage can be avoided, but the irregular oscillations in the phase-shift ratio are inevitable. Thus, the disturbances of the phase-shift ratio ΔPSR caused by the measurement noises should be treated as a criterion to evaluate the stability of the I^{2}ACL dc-dc converter. Then, the disturbance of required transferred current Δi^*_T caused by the measurement noise of output voltage U_{om} can be expressed as,

$$\Delta i^*_T = U_{om}(k_i + k_p) i^*_o \tag{7}$$

where k_i is the integral parameter and k_p is the proportional parameter of the PI controller. Then, based on the relationship between the transferred power and the phase-shift ratio of I^{2}ACL dc-dc converter, the disturbance of phase-shift ratio ΔPSR can be obtained by using the required transferred current i^*_T and its disturbance Δi^*_T as,

$$\Delta\text{PSR} = f(\Delta i^*_T, i^*_T) \le \Delta\text{PSR}_{\text{limt}} \tag{8}$$

where $\Delta\text{PSR}_{\text{limt}}$ is the limited value of the disturbance of phase-shift ratio caused by the measurement noise of the output voltage. Combining (7) and (8), k_i and k_p should meet the requirement as,

$$k_i + k_p \le \frac{U_{om} i^*_o}{f^{-1}(\Delta\text{PSR}_{\text{limt}}, i^*_T)} \tag{9}$$

Then, according to (9), the upper limitation of k_i and k_p can be obtained, and then, the disturbance of the phases-shift ratio can be restricted.

D. THE COMPENSATION OPERATION FOR THE EFFICIENCY DIFFERENCE CAUSED BY THE POWER LOSS

In the proposed general fast-dynamic control scheme, the PI controller is employed to compensate the difference between the transferred current i_T and the output current i_o caused by the power loss, and the efficiency η of the I^{2}ACL dc-dc converter can be approximatively expressed as,

$$\eta \approx \frac{P_o}{P_T} = \frac{U_o i_o}{U_o i_T} = \frac{1}{k_{io}} \tag{10}$$

According to (10), when the efficiency η of the new steady-state condition is a little different from its previous value, the new compensation coefficient k_{io} should also be a little different from its previous value. Then, when the input voltage and load condition are changed, more time is needed for obtaining the required coefficient k_{io} based on the PI controller. Therefore, to reduce the settling time under the general fast-dynamic control scheme, a general compensation method is proposed for the I^{2}ACL dc-dc converter. As shown in Fig. 42, the relationship among the transferred current i_T, the capacitor

charging current i_{Co}, and the load current i_o can always be expressed as,

$$i_{Co} = i_T - i_o \tag{11}$$

Moreover, with the output capacitor C_o, the output voltage of the I^{2}ACL dc-dc converter can be kept at its desired voltage in the previous switching periods after the variation of the input voltage or the load resistor. Therefore, when the capacitor charging current i_{Co} is not equivalent to zero, the transferred current i_T of the I^{2}ACL dc-dc converter should compensate for this capacitor current i_{Co}. Then, the transferred current i_T can be expressed as,

$$i_T = k_{io} i_o - i_{Co} = k_{io} i_o - \frac{C_o}{T_s}(U_o - U_o') \tag{12}$$

here U'_o is the measured output voltage in the last switching period. Then, the required compensation coefficient can be expressed as,

$$k'_{io} = \frac{1}{i_o}\left[k_{io} i_o - \frac{C_o}{T_s}(U_o - U_o')\right] \tag{13}$$

Then, when the load current i_o or the input voltage U_{in} is changed, (13) can be used to calculate the required compensation coefficient k_{io} for dealing with the efficiency difference under different conditions for the I^{2}ACL dc-dc converter. Moreover, as shown in Fig. 37, the current status of the inductance will change when the load current is changed, and according to (1), the additional power from the inductance is transferred to the output side. Then, (12) will become inaccurate, and the expected transferred current of the unidirectional I^{2}ACL dc-dc converter will also become inaccurate. Therefore, the compensation operation should be used after several switching periods until the peak value of the inductance current becomes stable. In addition, in the actual converter system, the measurement noise is unavoidable. To calculate the capacitor charging current i_{Co} more accurately, (13) should be further expressed as,

$$k'_{io} = \frac{1}{i_o}\left[k_{io} i_o - \frac{\sum_{j=1}^{m} \frac{C_o}{T_s}(U_{oj} - U'_{oj})}{m}\right] \tag{14}$$

Based on the compensation method, the influence caused by the efficiency difference will be reduced. Moreover, it can also be employed to reduce the influence caused by middle inductive energy release for unidirectional I^{2}ACL isolated dc-dc converter.

E. THE IMPLEMENTING PROCEDURES OF THE UNIFIED FDDC CONTROL SCHEME FOR I^{2}ACL-TYPE CONVERTER

In previous parts, the general FDDC control scheme is proposed for the I^{2}ACL isolated dc-dc converters. Then, the design principle of PI parameters and the compensation method for ensuring the performance of the unified method is also presented. Based on these contents, the detailed implementing procedures of the unified FDDC control scheme for arbitrary I^{2}ACL isolated dc-dc converter are demonstrated as shown in Fig. 43.

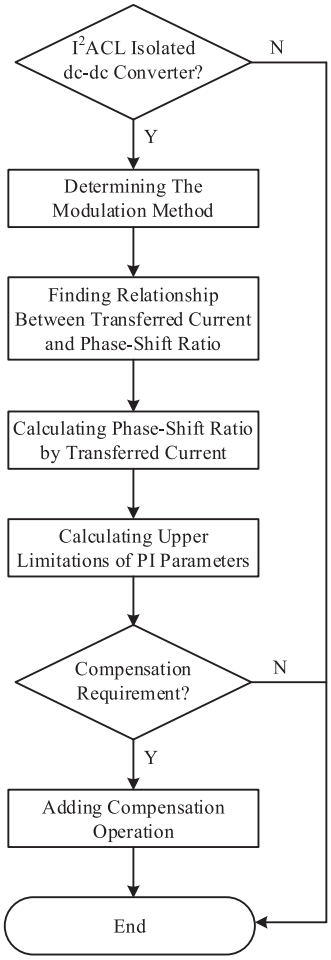

FIGURE 43. The implementing procedures of the unified FDDC control scheme for I^{2}ACL-type isolated dc-dc converter.

If the simplified circuit of an existing isolated dc-dc converter can be simplified as shown in Fig. 11 or Fig. 22, this converter can be classified as the I^{2}ACL isolated dc-dc converter. Then, the modulation method of this converter should be determined, and generally, the phase-shift modulation method is the most suitable modulation method for the I^{2}ACL converter. Based on the employed phase-shift modulation method, the relationship between the transferred current and the phase-shift ratio should be determined, which can be usually found in the existing papers [20], [22], [30], [37]. Moreover, to realize the proposed unified FDDC control scheme, the phase-shift ratio should be calculated by the transferred current, which can be employed to connect the outer-loop control value and the phase-shift ratio as shown in Fig. 41. Further, according to (9), the upper limitations of the PI parameters can be determined. Then, the proposed unified FDDC control scheme can be obtained for this specific I^{2}ACL isolated dc-dc converter. Sometimes, the I^{2}ACL dc-dc converter may perform at many different efficiencies under different loading conditions, which will influence the dynamic performance of the proposed scheme a little, especially for the unidirectional I^{2}ACL dc-dc converter. So, the presented

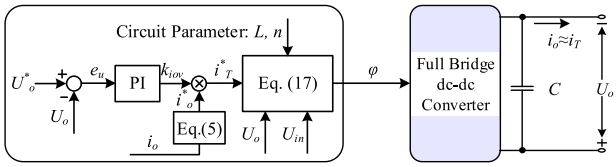

FIGURE 44. The control block of the FDDC scheme for the full-bridge dc-dc converter.

compensation operation as shown in Part D can be employed to reduce this influence, which is based on the disturbance of output-capacitor voltage. Finally, the implementing procedures of the proposed FDDC control scheme can be employed to a specific I^2ACL dc-dc converter.

IV. SIMULATION AND EXPERIMENT VERIFICATION

In this Section, by using some popular I^2ACL dc-dc converters including full-bridge dc-dc converter, DAB dc-dc converter, and three-phase DAB dc-dc converter as examples, the proposed unified FDDC control strategy will be verified.

A. EXPERIMENT RESULTS OF FULL-BRIDGE DC-DC CONVERTER

For the full-bridge dc-dc converter, the transferred current I_T can be calculated as,

$$I_T = \begin{cases} \frac{(k-1)U_{in}(1-d)^2T_s}{4nL} \left(\frac{k-1}{k} < d \le 1\right) \\ \frac{U_{in}(1-d^2)T_s}{8nL} - \frac{U_o^2T_s}{8n^3U_{in}L} \left(0 \le d \le \frac{k-1}{k}\right) \end{cases} \tag{15}$$

According to (15), the transferred current I_T of the FB dc-dc converter is not monotone decreasing along with the increasing of the phase-shift ratio d. To design the control system simply, a middle variable φ can be employed to replace the phase-shift d as,

$$d = 1 - \varphi \tag{16}$$

Then, the positive correlation between φ and I_T can be calculated as,

$$I_T = \begin{cases} \frac{(k-1)U_{in}\varphi^2T_s}{4nL} \left(0 \le \varphi \le \frac{1}{k}\right) \\ \frac{U_{in}\varphi(2-\varphi)T_s}{8nL} - \frac{U_o^2T_s}{8n^3U_{in}L} \left(\frac{1}{k} < \varphi \le 1\right) \end{cases} \tag{17}$$

According to (17), the required middle variable φ for the certain transferred current can be shown as,

$$\varphi = \begin{cases} \sqrt{\frac{4nLI_T}{(k-1)U_{in}T_s}} \left(0 \le I_T \le \frac{(k-1)U_o^2T_s}{4n^3LU_{in}}\right) \\ 1 - \sqrt{1 - \frac{8nLI_T}{U_{in}T_s} - \frac{U_o^2}{n^2U_{in}^2}} \left(\frac{(k-1)U_o^2T_s}{4n^3LU_{in}} < I_T \le \frac{(n^2U_{in}^2 - U_o^2)U_oTs}{8n^3LU_{in}^2}\right) \end{cases} \tag{18}$$

Combining Fig. 41(b), (5) and (18), the FDDC control scheme for full-bridge dc-dc converter can be shown in Fig. 44.

Moreover, the circuit parameters of the full-bridge dc-dc converter can be shown in Table 1. As the analysis at Part A in Section III, the middle inductance of the unidirectional I^2ACL dc-dc converter will release the storage power during the

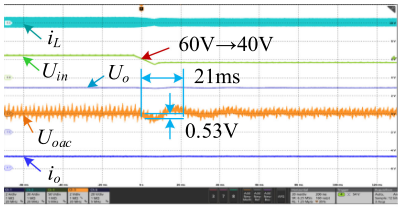

(a). The FDDC control strategy without compensation.

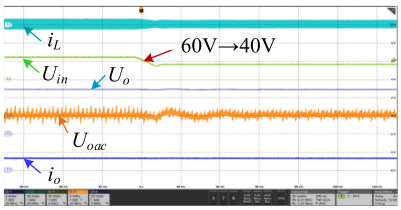

(b). The FDDC control strategy with compensation.

FIGURE 45. The experiment results when the input voltage is changed from 60 V to 40 V. (U_{in}: 50V/div; i_L: 30A/div; U_o: 20V/div; U_{oac}: 2V/div; i_o: 2A; t: 20 ms/div).

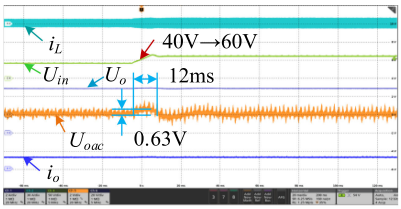

(a). The FDDC control strategy without compensation.

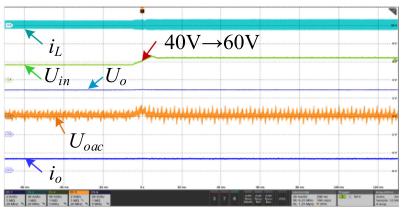

(b). The FDDC control strategy with compensation.

FIGURE 46. The experiment results when the input voltage is changed from 40 V to 60 V. (U_{in}: 50V/div; i_L: 30A/div; U_o: 20 V/div; U_{oac}: 2V/div; i_o: 2A; t: 20 ms/div).

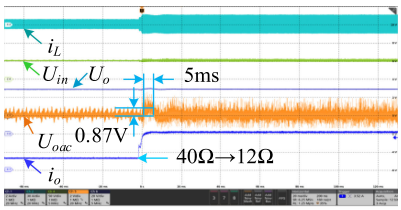

(a). The FDDC control strategy without compensation.

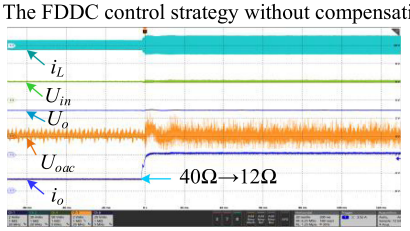

(b). The FDDC control strategy with compensation.

FIGURE 47. The experiment results when the load resistor is changed from 40 Ωto 12Ω. (U_{in}: 50V/div; i_L: 30A/div; U_o: 20V/div; U_{oac}: 2V/div; i_o: 2A; t: 20 ms/div).

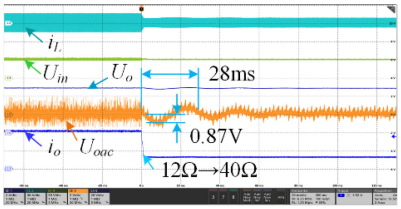

(a). The FDDC control strategy without compensation.

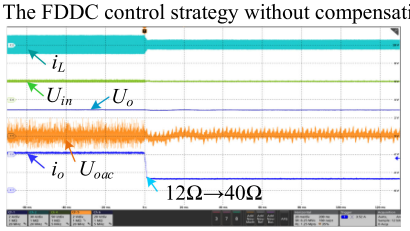

(b). The FDDC control strategy with compensation.

FIGURE 48. The experiment results when the load resistor is changed from 12 Ωto 40Ω. (U_{in}: 50V/div; i_L: 30A/div; U_o: 20V/div; U_{oac}: 2V/div; i_o: 2A; t: 20 ms/div).

TABLE 1. Circuit Parameters of The Full Bridge DC-DC Converter

Switches	SCT3080
L	50μH
n	2
f_s	10kHz
U^*_o	50V
C_o	1mF
R	12Ω or 40Ω
k_p, k_i	0.05, 0.005

transient process, which may influence the dynamic performance. So, for the full-bridge dc-dc converter, the experiment result under the FDDC control strategy without or with the compensation operation as shown in Part D in Section III will be provided. Then based on the FDDC control scheme, the corresponding experiment results when the input voltage and the load resistor of the full-bridge dc-dc converter are changed can be shown as Fig. 45–Fig. 47, and Fig. 48, respectively.

When the load resistor R is selected as 40 Ω, the experiment results under the FDDC control scheme without compensation operation and the FDDC control scheme with compensation operation when the input voltage U_{in} is changed between 40 V and 60 V can be shown in Fig. 45 and Fig. 46. As shown in Fig. 45(a) and Fig. 46(a), when the input voltage is changed, the output-voltage disturbances under the FDDC control scheme without compensation operation are bigger than 0.5 V, and the settling times are obvious. Then, with compensation operation, the output-voltage disturbances under the FDDC control scheme when the input voltage is changed are very small, and the settling times can be omitted as shown in Fig. 45(b) and Fig. 46(b).

In addition, when the input voltage U_{in} is selected as 50 V, the experiment results under the FDDC control scheme without compensation operation and the FDDC control scheme with compensation operation when the load resistor R is changed between 12 Ωand 40 Ωcan be shown in Fig. 47 and Fig. 48. As shown in Fig. 47(a) and Fig. 48(a), when the load resistor is changed, the output-voltage disturbances under the

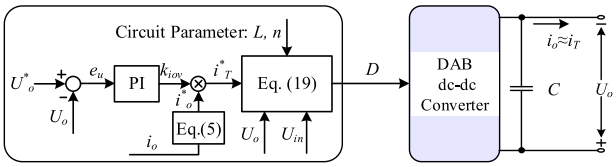

FIGURE 49. The control block of the FDDC scheme for the DAB dc-dc converter.

TABLE 2. Circuit Parameters of The DAB DC-DC Converter System

Switches (Experiment platform)	SCT3080KL
L	50 μH
n	2
f_s	10 kHz
R	20 Ω ~ 100 Ω
U_{in}	40 V ~ 50 V
U^*_o	80 V
k_p	0.05
k_i	0.005

FDDC control scheme without compensation operation are bigger than 0.8 V, and the settling times are obvious. Then, with compensation operation, the output-voltage disturbances under the FDDC control scheme when the load resistor is changed are very small, and the settling times can be omitted as shown in Fig. 47(b) and Fig. 48(b).

B. EXPERIMENT RESULTS OF DAB DC-DC CONVERTER

For the DAB dc-dc converter, the transferred current I_T under the single-phase-shift modulation method can be expressed by the phase-shift ratio D as,

$$I_T = \frac{U_{in}D(1-D)T_s}{2nL}\left(0 \le D \le \frac{1}{2}\right) \tag{19}$$

Then, the phase-shift ratio D of the DAB dc-dc converter can also be calculated by the transferred current as,

$$D = \frac{1}{2} - \sqrt{\frac{1}{4} - \frac{2nLI_T}{U_{in}T_s}}\left(0 \le I_T \le \frac{U_{in}T_s}{8nL}\right) \tag{20}$$

Combining Fig. 40(b), (5) and (20), the FDDC scheme for the DAB dc-dc converter can be shown in Fig. 49.

Moreover, the circuit parameters of the DAB dc-dc converter can be shown in Table 2. Since DAB dc-dc converter can usually illustrate high efficiency for a large power range, the FDDC scheme is enough for ensuring the fast-dynamic performance when the input voltage and the load resistor are changed. Then based on the FDDC control scheme for DAB dc-dc converter, the corresponding experiment results when the input voltage and the load resistor of the DAB dc-dc converter are changed can be shown as Fig. 50.

When the load resistor R is 20 Ω, the experiment results under the FDDC control scheme when the input voltage U_{in} is changed between 40 V to 50 V can be shown as Fig. 50(a) and Fig. 50(b), where the output voltage can be kept at its desired value. Moreover, when the input voltage U_{in} is 40 V, the experiment results under the FDDC control scheme when the load resistor R is changed between 20 Ωand 100 Ωcan be

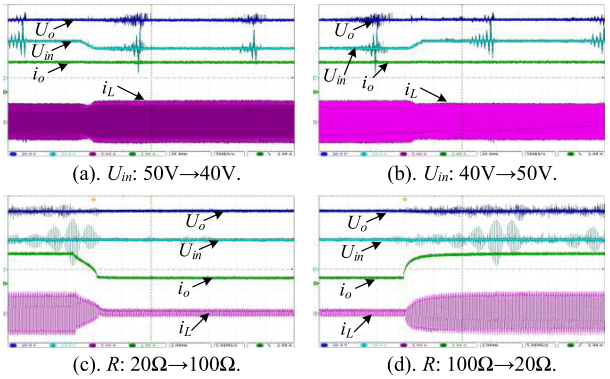

(a). U_{in}: 50V→40V. (b). U_{in}: 40V→50V.

(c). R: 20Ω→100Ω. (d). R: 100Ω→20Ω.

FIGURE 50. The experiment result under FDDC control scheme for DAB dc-dc converter. (U_{in} and U_o: 20V/div; i_o: 2A/div; i_L: 5A/div; t: 2ms/div).

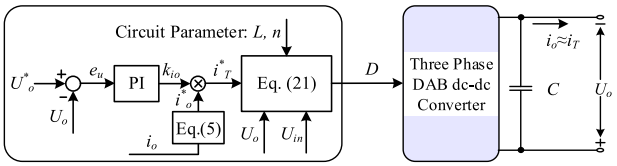

FIGURE 51. The control block of the FDDC scheme for the three-phase DAB dc-dc converter.

shown as Fig. 50(c) and Fig. 50(d), where the output-voltage disturbance can be neglected. Therefore, based on the general FDDC control scheme, an excellent dynamic control scheme can be provided for the DAB dc-dc converter when the input voltage and the load resistor are changed.

C. SIMULATION RESULTS OF THREE-PHASE DAB DC-DC CONVERTER

For the three-phase dc-dc converter, the transferred current I_T under the single-phase-shift modulation method can be expressed by the phase-shift ratio D as,

$$I_T = \begin{cases} \frac{U_{in}T_s}{2nL}(\frac{2}{3} - \frac{D}{2})D(0 \le D < \frac{1}{3}) \\ \frac{U_{in}T_s}{2nL}[D(1-D) - \frac{1}{18}](\frac{1}{3} \le I_T \le \frac{1}{2}) \end{cases} \tag{21}$$

Then, the phase-shift ratio D of the three-phase DAB dc-dc converter can also be calculated by the transferred current as,

$$D = \begin{cases} \frac{2}{3} - \sqrt{\frac{4}{9} - \frac{4nLI_T}{U_{in}T_s}}(0 \le I_T < \frac{U_{in}T_s}{12nL}) \\ \frac{1}{2} - \sqrt{\frac{14}{72} - \frac{2nLI_T}{U_{in}T_s}}(\frac{U_{in}T_s}{12nL} \le I_T \le \frac{7U_{in}T_s}{72nL}) \end{cases} \tag{22}$$

Combining Fig. 40(b), (5) and (22), the FDDC scheme for the three-phase DAB dc-dc converter can be shown in Fig. 51.

Moreover, the circuit parameters of the three-phase DAB dc-dc converter can be shown in Table 3. Since three-phase DAB dc-dc converter can usually have high efficiency for a large power range, the FDDC scheme is enough for ensuring the fast-dynamic performance when the input voltage and the load resistor are changed. Then, based on the FDDC control scheme for the three-phase DAB dc-dc converter, the corresponding experiment results when the input voltage and the load resistor of the three-phase DAB dc-dc converter are changed can be shown as Fig. 52 and Fig. 53, respectively.

TABLE 3. Circuit Parameters of The Three Phase DAB DC-DC Converter

Switches	SCT3080
L	50μH
n	1
f_s	10kHz
U_{in}	100V~120V
U^*_o	100V
C_o	2mF
R	12Ω~200Ω
U_m (Measurement noise in voltages)	±0.5V
R_{on} (Conduction resistor in switch)	50mΩ
k_p, k_i	0.1, 0.01

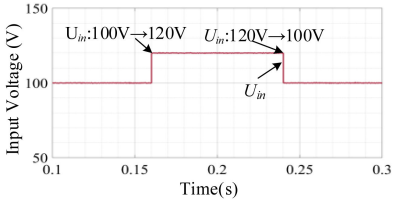

(a). Input voltage.

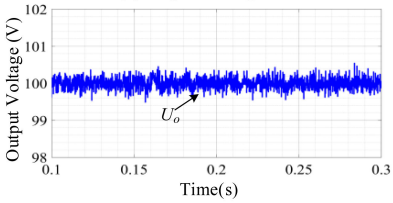

(b). Output voltage.

FIGURE 52. The simulation result when the input voltage is changed between 100 V and 120 V.

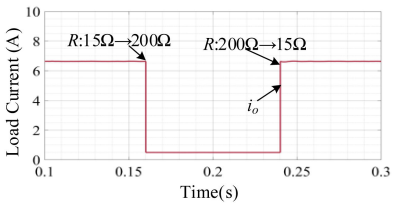

(a). Load current.

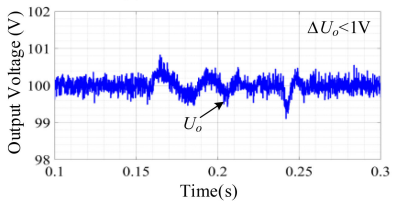

(b). Output voltage.

FIGURE 53. The simulation result when the load resistor is changed from 15 Ωto 200Ω.

When the load resistor R is 12 Ω, the experiment results under the FDDC control scheme when the input voltage U_{in} of the three-phase DAB dc-dc converter is changed between 100 V to 120 V can be shown as Fig. 52, where the output voltage can be kept at its desired value. Moreover, when the input voltage U_{in} is 100 V, the experiment results under the FDDC control scheme when the load resistor R of the three-phase DAB dc-dc converter is changed between 15 Ωand 200 Ωcan be shown as Fig. 53, where the output-voltage disturbance

is smaller than 1 V. Therefore, based on the general FDDC control scheme, an excellent dynamic control scheme can be provided for the three-phase DAB dc-dc converter when the input voltage and the load resistor are changed.

V. CONCLUSION

In this paper, the isolated dc-dc converters with intermediary inductive ac-link are reviewed since these converters have similar transient characteristics. These converters are divided into two groups including the unidirectional type and the bidirectional type. Then, the current transferred characteristics of these converters are analyzed, which reveals the order reducing phenomena since the intermediary inductance cannot influence the transient performance. Moreover, a unified fast-dynamic direct-current control scheme is proposed for providing excellent dynamic performance for this kind of dc-dc converters with time-varying input voltage and load conditions. Moreover, the design principle of PI parameters in the proposed method is presented, and the compensation operation is also provided for ensuring fast-dynamic performance. Based on the review of the intermediary inductive ac-link isolated dc-dc converter and the proposed general fast-dynamic control scheme, the conducted studies are summarized as follows:

1) A thorough overview has been done for intermediary inductive ac-link isolated dc-dc converters with clear classifications, which reveals the fundamental dynamic equivalence among various dc-dc converters. Such common features can be found not only in existing topologies, but also in undiscovered new topologies from the same dc-dc converter family.
2) By using the full-bridge dc-dc converter and the dual-active-bridge dc-dc converter as examples, the power transferred performances of the unidirectional and bidirectional middle inductive ac-link isolated dc-dc converters are analyzed, respectively.
3) The proposed general fast-dynamic direct-current control scheme can provide an excellent dynamic response for intermediary inductive ac-link isolated dc-dc converter when the input voltage and the load condition are changed. Moreover, the presented principle for designing the PI parameter in the general fast-dynamic control scheme can ensure the stability of the converter system. The dynamic equivalence of these intermediary inductive ac-link isolated dc-dc converter is also verified.

REFERENCES

[1] H. Cha, R. Ding, Q. Tang, and F. Z. Peng, "Design and development of high-power DC–DC converter for metro vehicle system," *IEEE Trans. Ind. Appl.*, vol. 44, no. 6, pp. 1795–1804, Nov./Dec. 2008.

[2] N. M. L. Tan, S. Inoue, A. Kobayashi, and H. Akagi, "Voltage balancing of a 320-V, 12-F electric double-layer capacitor bank combined with a 10-kW bidirectional isolated DC–DC converter," *IEEE Trans. Power Electron.*, vol. 23, no. 6, pp. 2755–2765, Nov. 2008.

[3] H. Plesko, J. Biela, J. Luomi, and J. W. Kolar, "Novel concepts for integrating the electric drive and auxiliary DC–DC converter for hybrid vehicles," *IEEE Trans. Power Electron.*, vol. 23, no. 6, pp. 3025–3034, Nov. 2008.

[4] F. Krismer and J. W. Kolar, "Efficiency-optimized high-current dual active bridge converter for automotive applications," *IEEE Trans. Ind. Electron.*, vol. 59, no. 7, pp. 2745–2760, Jul. 2012.

[5] D. Rothmund, T. Guillod, D. Bortis, and J. W. Kolar, "99% Efficient 10 kV sic-Based 7 kV/400 v DC transformer for future data centers," *IEEE J. Emerg. Sel. Top. Power Electron.*, vol. 7, no. 2, pp. 753–767, Jun. 2019.

[6] B. Zhao, Q. Song, W. Liu, and Y. Sun, "Overview of dual-active-bridge isolated bidirectional DC–DC converter for high-frequency-link power-conversion system," *IEEE Trans. Power Electron.*, vol. 29, no. 8, pp. 4091–4106, Aug. 2014.

[7] N. Hou and Y. W. Li, "Overview and comparison of modulation and control strategies for a nonresonant single-phase dual-active-bridge DC–DC converter," *IEEE Trans. Power Electron.*, vol. 35, no. 3, pp. 3148–3172, Mar. 2020.

[8] S. Inoue and H. Akagi, "A bidirectional isolated DC–DC converter as a core circuit of the next-generation medium-voltage power conversion system," *IEEE Trans. Power Electron.*, vol. 22, no. 2, pp. 535–542, Mar. 2007.

[9] M. Kwon and S. Choi, "Control scheme for autonomous and smooth mode switching of bidirectional DC–DC converters in a DC microgrid," *IEEE Trans. Power Electron.*, vol. 33, no. 8, pp. 7094–7104, Aug. 2018.

[10] N. Hou and Y. Li, "The comprehensive circuit-parameter estimating strategies for output-parallel dual-active-bridge DC–DC converters with tunable power sharing control," *IEEE Trans. Ind. Electron.*, vol. 67, no. 9, pp. 7583–7594, Sep. 2020.

[11] J. Liu, J. Yang, J. Zhang, Z. Nan, and Q. Zheng, "Voltage balance control based on dual active bridge DC/DC converters in a power electronic traction transformer," *IEEE Trans. Power Electron.*, vol. 33, no. 2, pp. 1696–1714, Feb. 2018.

[12] L. Wang, Q. Zhu, W. Yu, and A. Q. Huang, "A medium-voltage medium-frequency isolated DC–DC converter based on 15-kV SiC MOSFETs," *IEEE J. Emerg. Sel. Top. Power Electron.*, vol. 5, no. 1, pp. 100–109, Mar. 2017.

[13] H. Tarzamni, F. P. Esmaeelnia, M. Fotuhi-Firuzabad, F. Tahami, S. Tohidi, and P. Dehghanian, "Comprehensive analytics for reliability evaluation of conventional isolated multiswitch PWM DC–DC converters," *IEEE Trans. Power Electron.*, vol. 35, no. 5, pp. 5254–5266, May 2020.

[14] S. A. Gorji, H. G. Sahebi, M. Ektesabi, and A. B. Rad, "Topologies and control schemes of bidirectional DC–DC power converters: An overview," *IEEE Access*, vol. 7, pp. 117997–118019, 2019.

[15] X. Pan, H. Li, Y. Liu, T. Zhao, C. Ju, and A. K. Rathore, "An overview and comprehensive comparative evaluation of current-fed-isolated-bidirectional DC/DC converter," *IEEE Trans. Power Electron.*, vol. 35, no. 3, pp. 2737–2763, Mar. 2020.

[16] A. Chub, D. Vinnikov, F. Blaabjerg, and F. Z. Peng, "A review of galvanically isolated impedance-source DC–DC converters," *IEEE Trans. Power Electron.*, vol. 31, no. 4, pp. 2808–2828, Apr. 2016.

[17] Y. Xie, R. Ghaemi, J. Sun, and J. S. Freudenberg, "Implicit model predictive control of a full bridge DC-DC converter," *IEEE Trans. Power Electron.*, vol. 24, no. 12, pp. 2704–2713, Dec. 2009.

[18] R. W. A. A. De Doncker, D. M. Divan, and M. H. Kheraluwala, "A three-phase soft-switched high-power-density DC/DC converter for high-power applications," *IEEE Trans. Ind. Appl.*, vol. 27, no. 1, pp. 63–73, Jan. 1991.

[19] A. J. B. Bottion and I. Barbi, "Input-Series and output-series connected modular output capacitor full-bridge PWM DC–DC converter," *IEEE Trans. Ind. Electron.*, vol. 62, no. 10, pp. 6213–6221, Oct. 2015.

[20] C. Zhao, S. D. Round, and J. W. Kolar, "An isolated three-port bidirectional DC-DC converter with decoupled power flow management," *IEEE Trans. Power Electron.*, vol. 23, no. 5, pp. 2443–2453, Sep. 2008.

[21] L. Wang, D. Zhang, Y. Wang, B. Wu, and H. S. Athab, "Power and voltage balance control of a novel three-phase solid-state transformer using multilevel cascaded H-Bridge inverters for microgrid applications," *IEEE Trans. Power Electron.*, vol. 31, no. 4, pp. 3289–3301, Apr. 2016.

[22] J. Hu, Z. Yang, S. Cui, and R. W. De Doncker, "Closed-form asymmetrical duty-cycle control to extend the soft-switching range of three-phase dual-active bridge converters," *IEEE Trans. Power Electron.*, vol. 36, no. 8, pp. 9609–9622, Aug. 2021.

[23] M. Sharifzadeh, H. Vahedi, A. Sheikholeslami, P. Labbé, and K. Al-Haddad, "Hybrid SHM–SHE modulation technique for a four-leg NPC inverter with DC capacitor self-voltage balancing," *IEEE Trans. Ind. Electron.*, vol. 62, no. 8, pp. 4890–4899, Aug. 2015.
[24] D. G. Bandeira, T. B. Lazzarin, and I. Barbi, "High voltage power supply using a T-Type parallel resonant DC–DC converter," *IEEE Trans. Ind. Appl.*, vol. 54, no. 3, pp. 2459–2470, May/Jun. 2018.
[25] A. Filba-Martinez, S. Busquets-Monge, and J. Bordonau, "Modulation and capacitor voltage balancing control of multilevel NPC dual active bridge DC–DC converters," *IEEE Trans. Ind. Electron.*, vol. 67, no. 4, pp. 2499–2510, Apr. 2020.
[26] Y. Li, Y. W. Li, H. Tian, N. R. Zargari, and Z. Cheng, "A modular design approach to provide exhaustive carrier-based PWM patterns for multilevel ANPC converters," *IEEE Trans. Ind. Appl.*, vol. 55, no. 5, pp. 5032–5044, Sep.–Oct. 2019.
[27] R. Suryadevara and L. Parsa, "Full-bridge ZCS-converter-based high-gain modular DC-DC converter for PV integration with medium-voltage DC grids," *IEEE Trans. Energy Convers.*, vol. 34, no. 1, pp. 302–312, Mar. 2019.
[28] X. Kong and A. M. Khambadkone, "Analysis and implementation of a high efficiency, interleaved current-fed full bridge converter for fuel cell system," *IEEE Trans. Power Electron.*, vol. 22, no. 2, pp. 543–550, Mar. 2007.
[29] J. Saeed and A. Hasan, "Unit prediction horizon binary search-based model predictive control of full-bridge DC–DC converter," *IEEE Trans. Control Syst. Technol.*, vol. 26, no. 2, pp. 463–474, Mar. 2018.
[30] N. Hou and Y. Li, "A direct current control scheme with compensation operation and circuit-parameter estimation for full-bridge DC–DC converter," *IEEE Trans. Power Electron.*, vol. 36, no. 1, pp. 1130–1142, Jan. 2021.
[31] N. C. D. Pont, D. G. Bandeira, T. B. Lazzarin, and I. Barbi, "A ZVS APWM half-bridge parallel resonant DC–DC converter with capacitive output," *IEEE Trans. Ind. Electron.*, vol. 66, no. 7, pp. 5231–5241, Jul. 2019.
[32] H. Wu, Y. Lu, T. Mu, and Y. Xing, "A family of soft-switching DC–DC converters based on a phase-shift-controlled active boost rectifier," *IEEE Trans. Power Electron.*, vol. 30, no. 2, pp. 657–667, Feb. 2015.
[33] Y. Xie, R. Ghaemi, J. Sun, and J. S. Freudenberg, "Model predictive control for a full bridge DC/DC converter," *IEEE Trans. Control Syst. Technol.*, vol. 20, no. 1, pp. 164–172, Jan. 2012.
[34] R. Huang and S. K. Mazumder, "A soft switching scheme for multi-phase DC/Pulsating-DC converter for three-phase high-frequency-link pulsewidth modulation (PWM) inverter," *IEEE Trans. Power Electron.*, vol. 25, no. 7, pp. 1761–1774, Jul. 2010.
[35] K. Nguyen-Duy, Z. Ouyang, L. P. Petersen, A. Knott, O. C. Thomsen, and M. A. E. Andersen, "Design of a 300-W isolated power supply for ultrafast tracking converters," *IEEE Trans. Power Electron.*, vol. 30, no. 6, pp. 3319–3333, Jun. 2015.
[36] Y. Li, F. Li, F. Zhao, and X. You, "Variable-Frequency control strategy of isolated buck–boost converter," *IEEE J. Emerg. Sel. Top. Power Electron.*, vol. 7, no. 3, pp. 1824–1836, Sep. 2019.
[37] D. Sha, D. Chen, S. Khan, and Z. Guo, "Voltage-Fed three-phase semi-dual active bridge DC–DC converter utilizing varying operating modes with high conversion efficiency," *IEEE Trans. Power Electron.*, vol. 34, no. 10, pp. 9447–9458, Oct. 2019.
[38] Z. Li, S. Dusmez, and H. Wang, "A novel soft-switching secondary-side modulated multioutput DC–DC converter with extended ZVS range," *IEEE Trans. Power Electron.*, vol. 34, no. 1, pp. 106–116, Jan. 2019.
[39] Y. Lu, H. Wu, B. Tu, M. Li, Y. Xia, and Y. Xing, "Ultra-Wide output voltage range power supply based on modular switched-converter principle," *IEEE Trans. Power Electron.*, vol. 35, no. 1, pp. 94–106, Jan. 2020.
[40] S. S. Williamson, A. K. Rathore, and F. Musavi, "Industrial electronics for electric transportation: Current State-of-the-Art and future challenges," *IEEE Trans. Ind. Electron.*, vol. 62, no. 5, pp. 3021–3032, May 2015.
[41] G. Ortiz, D. Bortis, J. Biela, and J. W. Kolar, "Optimal design of a 3.5-kV/11-kW DC–DC converter for charging capacitor banks of power modulators," *IEEE Trans. Plasma Sci.*, vol. 38, no. 10, pp. 2565–2573, Oct. 2010.
[42] M. S. Irfan, A. Ahmed, J. Park, and C. Seo, "Current-Sensorless power-decoupling phase-shift dual-half-bridge converter for DC–AC power conversion systems without electrolytic capacitor," *IEEE Trans. Power Electron.*, vol. 32, no. 5, pp. 3610–3622, May 2017.
[43] J. Wang, F. Z. Peng, J. Anderson, A. Joseph, and R. Buffenbarger, "Low cost fuel cell converter system for residential power generation," *IEEE Trans. Power Electron.*, vol. 19, no. 5, pp. 1315–1322, Sep. 2004.
[44] R. W. De Doncker, D. M. Divan, and M. H. Kheraluwala, "A three-phase soft-switched high power density DC/DC converter for high power applications," in *Conf. Rec. 1988 IEEE Ind. Appl. Soc. Annu. Meeting*, Pittsburgh, PA, USA, 1988, pp. 796–805.
[45] J. Hu, S. Cui, S. Wang, and R. W. De Doncker, "Instantaneous flux and current control for a three-phase dual-active bridge DC–DC converter," *IEEE Trans. Power Electron.*, vol. 35, no. 2, pp. 2184–2195, Feb. 2020.
[46] H. M. de Oliveira Filho, D. de Souza Oliveira, and P. P. Praça, "Steady-State analysis of a ZVS bidirectional isolated three-phase DC–DC converter using dual phase-shift control with variable duty cycle," *IEEE Trans. Power Electron.*, vol. 31, no. 3, pp. 1863–1872, Mar. 2016.
[47] Demirel, O., U. Arifoglu, and K. Kalayci, "Novel three-level T-type isolated bidirectional DC–DC converter," *IET Power Electron.*, vol. 12, no. 1, pp. 61–71, 2018.
[48] S. B. Karanki and D. Xu, "NPC based dual active bridge topology for integrating battery energy storage to utility gird," in *proc. 2014 IEEE 27th Can. Conf. Elect. Comput. Eng. (CCECE)*, Toronto, ON, Canada, 2014, pp. 1–6.
[49] Y. Xuan, X. Yang, W. Chen, T. Liu, and X. Hao, "A novel NPC dual-active-bridge converter with blocking capacitor for energy storage system," *IEEE Trans. Power Electron.*, vol. 34, no. 11, pp. 10635–10649, Nov. 2019.
[50] R. M. Burkart and J. W. Kolar, "Comparative η–ρ–σ Pareto optimization of Si and SiC multilevel dual-active-bridge topologies with wide input voltage range," *IEEE Trans. Power Electron.*, vol. 32, no. 7, pp. 5258–5270, Jul. 2017.
[51] A. Filba-Martinez, S. Busquets-Monge, and J. Bordonau, "Modulation and capacitor voltage balancing control of multilevel NPC dual active bridge DC–DC converters," *IEEE Trans. Ind. Electron.*, vol. 67, no. 4, pp. 2499–2510, Apr. 2020.
[52] Jakka, V. N. S. R., A. Shukla, and G. Demetriades, "Three-winding transformer based asymmetrical dual active bridge converter," *IET Power Electron.*, vol. 9, no. 12, pp. 2377–2386, 2016.
[53] Teng, H., Y. Zhong, and H. Bai, "SiC+ Si three-phase 48 v electric vehicle battery charger employing current-SVPWM controlled SWISS AC/DC and variable-DC-bus DC/DC converters," *IET Elect. Syst. Transp.*, vol. 8, no. 4, pp. 231–239, 2018.
[54] W. Song, N. Hou, and M. Wu, "Virtual direct power control scheme of dual active bridge DC–DC converters for fast dynamic response," *IEEE Trans. Power Electron.*, vol. 33, no. 2, pp. 1750–1759, Feb. 2018.
[55] N. Hou and Y. Li, "Communication-Free power management strategy for the multiple DAB-Based energy storage system in islanded DC microgrid," *IEEE Trans. Power Electron.*, vol. 36, no. 4, pp. 4828–4838, Apr. 2021.

NIE HOU (Student Member, IEEE) received the B.S. and M.S. degrees in electrical engineering from Southwest Jiaotong University, Chengdu, China, in 2014 and 2017, respectively. He is currently working toward the Ph.D. degree with the Department of Electrical and Computer Engineering, University of Alberta, Edmonton, AB, Canada.

His current research interests include digital control and optimization methods of DC-DC converter and DC distribution system.

Mr. Hou was the recipient of the Outstanding Author Award from the Proceeding of the Chinese Society for Electrical Engineering in 2016.

YUZHUO LI (Student Member, IEEE) received the B.S. and M.S. degrees in control science and engineering from Shandong University, Jinan, China, in 2012 and 2015, respectively. Since 2015, he has been working toward the Ph.D. degree with the University of Alberta, Edmonton, AB, Canada.

His main research interests include systematic power converter topology derivation and PWM design.

ZHONGYI QUAN (Member, IEEE) was born in Taiyuan, Shanxi, China. He received the B.Sc. degree from Tianjin University, Tianjin, China, in 2010, the M.Sc. degree from Beihang University, Beijing, China, in 2013, and the Ph.D. degree in electrical engineering from the University of Alberta, Edmonton, AB, Canada, in 2019. He was a Postdoctoral Fellow with the University of Alberta. In 2019, he was also a Visiting Research Fellow with the Institute for Power Generation and Storage Systems (PGS), E.ON Energy Research Center, RWTH Aachen University, Aachen, Germany. He is also the founder and CEO of Electronic Grid Systems Inc. since 2020, a technology start-up based in Edmonton, Alberta, Canada. His research interests include design of high density and high efficiency power converters for applications, such as renewable energy, microgrids, electric vehicles, and other energy efficient equipment.

He was the recipient of the IEEE PELS ECCE Best Student Project Demonstration on Emerging Technology 3rd Prize Award in 2018, the Alberta GreenSTEM Fellowship in 2020, and the Best Paper Award in IPEMC 2020 (ECCE-Asia) in 2020.

YUN WEI LI (Fellow, IEEE) received the B.Sc. in Engineering degree in electrical engineering from Tianjin University, Tianjin, China, in 2002, and the Ph.D. degree from Nanyang Technological University, Singapore, in 2006.

In 2005, he was a Visiting Scholar with Aalborg University, Aalborg, Denmark. From 2006 to 2007, he was a Postdoctoral Research Fellow with Ryerson University, Toronto, ON, Canada. In 2007, he also with Rockwell Automation, Canada, before he joined the University of Alberta, Edmonton, AB, Canada in the same year. Since then, he has been with University of Alberta, where he is currently a Professor. His research interests include distributed generation, microgrid, renewable energy, high power converters, and electric motor drives.

He was the Editor-in-Chief of the IEEE TRANSACTIONS ON POWER ELECTRONICS LETTERS. Prior to that, he was an Associate Editor for the IEEE TRANSACTIONS ON POWER ELECTRONICS, IEEE TRANSACTIONS ON INDUSTRIAL ELECTRONICS, IEEE TRANSACTIONS ON SMART GRID, and IEEE JOURNAL OF EMERGING AND SELECTED TOPICS IN POWER ELECTRONICS. He was the recipient of the Richard M. Bass Outstanding Young Power Electronics Engineer Award from IEEE Power Electronics Society in 2013 and the Second Prize Paper Award of the IEEE TRANSACTIONS ON POWER ELECTRONICS in 2014.

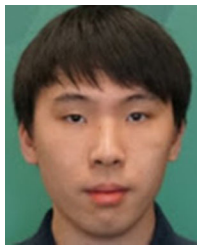

ANDREW ZHOU received the B.Sc. and M.Sc. degrees in electrical engineering from the University of Alberta, Edmonton, AB, Canada, in 2017 and 2021, respectively.

His research interests include renewable energy, wind energy conversion systems, low-voltage ride-through control, and control of power converters.